

# Cornering in the Water: An Investigation of Dolphin Swimming Performance

Mingkai Xia\*, Junhan Zhang\*, Ningshan Wang, Gabriel Antoniak, Nicole West, Ding Zhang, Kenneth Alex Shorter †

November 27, 2024

## Abstract

This article provides new insights into dolphin maneuver strategies in lap swimming tasks. However, most existing research focuses on straight-line swimming leaving the study of dolphins' cornering strategies an open area. Challenges for directly analyzing dolphins' turning behavior include difficulties in motion tracking underwater and the inability to directly measure the propulsive forces. This paper provides methodology and analyses of dolphins' swimming performance during lap swimming tasks. External camera detection and internal kinematics measured from wearable bio-tags are involved in this study to support accurate localization of the animals. A particle filter, which fuses the external and internal measurements, is implemented to provide accurate estimations of the trajectories, even when they swim deep below the water's surface. Thereafter, a hydrodynamic model is constructed to calculate the thrust power and energy cost of the animals. The energetic cost during lap swimming is calculated for the comparison between different cornering behaviors. The results show that the implemented particle filter can provide precise and complete trajectories of the tested dolphins, providing fundamental for statistical study of the cornering behavior. From the kinematic analysis, TT01 is the fastest lap swimmer, with the highest swimming speed for the whole lap while performing a sharp turn with small deceleration. TT02 performs greater energetic efficiency than TT01 by transferring more weight at high speed. TT03 shows the highest energetic efficiency by maintaining a slow underwater motion.

## 1 Introduction

Understanding and tracking the behavior of marine mammals is a significant area of research nowadays. Dolphins are known for their efficient swimming techniques Fish et al. [2014]. By studying how dolphins move and navigate through water, we can gain valuable insights that can inspire the development of innovative bio-inspired robots and enhance their control methods. [Yu et al., 2019] implements a control method enabling a robotic dolphin to perform repetitive leaping at the water's surface. [Li et al., 2024] develops an integrated robotic dolphin and a robust motion control system capable of operating in complex underwater environments.

Engineering researchers also learn from dolphin movements to develop energy-saving strategies for navigation. [Fish and Rohr, 1999] demonstrates that although dolphins rarely move in a straight line, the fluking motion returns the body to a stable straight position during underwater movement. Thus most biomechanics analysis studies related to dolphins have been focused on straight-line swimming. [Antoniak et al., 2023] investigates the propulsive efficiency during steady-state swimming using a hydro-elasticity model. Studies on energetic costs in animals extend beyond the examination of straight-line motion. Notably, [Wilson et al., 2021] suggests that land animals may work to minimize movement costs by reducing their speed in response to increased path variability. However, research on the energetic costs associated with dolphin maneuverability and turning is challenging and remains an open area of study.

A significant challenge is the real-time localization of dolphins' trajectories while they swim underwater. Commonly employed strategies include overhead cameras [Gabaldon et al., 2022a] and wearable sensors [Kaidarova et al., 2023]. Although the data from wearable sensors offers high-fidelity kinematic information which can be utilized to construct complete dead-reckoning tracks [Wensveen et al., 2015], the principle of dead-reckoning determines that the result accuracy would be compromised by the accumulation of sensor drift. On the other hand, cameras provide reliable positions for dolphins, but they fail to capture dolphin movements when the dolphins dive deep or when excessive sunlight creates reflections on the water's surface. Consequently, the trajectory generated by camera detection can be too sparse for kinematic analysis. This issue can be resolved by the fusion of the data from camera and wearable sensors. See [Gabaldon et al., 2017, Zhang et al., 2019].

Another challenge for field tests is to obtain propulsive force and power. The nature of fluking determines that the direct measurements of force and power for marine mammals are difficult. Therefore, it is essential to first establish a dynamic model. Once this model is in place, kinematic data from the wearable sensor can be utilized to estimate the kinetics and energetics associated with the dolphin's turning behavior and maneuverability for underwater swimming. See [Zhang et al., 2023, Gabaldon et al., 2022b, Fish, 1993].

In this article, we integrate a robust localization technique with a tag-based biomechanics analysis to comprehensively characterize, predict, describe, and explain movement patterns during a prescribed swimming task involving a 180-degree change in heading. The data is

\*The two authors have equal contributions in this paper.

†Corresponding author: Associate professor, Mechanical Engineering, University of Michigan, 2350 Hayward, Ann Arbor, MI 48109, kshorter@umich.edu

collected from three tested dolphins: TT01, TT02, and TT03. A Faster R-CNN detector [Ren et al., 2016] is trained and verified using overhead video. After camera calibration, the detection is transformed into the world reference frame using a perspective transformation homography [Hartley, 1997]. A bio-tag is attached to the dolphin to record the depth, longitudinal water speed, and attitude. The tangential acceleration, normal acceleration, power consumption, and cost of transport (COT) are further calculated by applying the collected kinematics. A dynamic model of the dolphin is constructed based on the work of [Gabaldon et al., 2022b] to obtain propulsive force. Speed and power are normalized with the dolphin’s body length and mass, allowing comparison of different dolphins’ swimming strategies. A particle filter is implemented to integrate the camera detection and tag measurement to form a complete trajectory of the dolphin during the lap trials and is further used to analyze the dolphin swimming performance in cornering. The swimming behavior of dolphins is analyzed using kinematic variables and trajectory data to identify the best lap swimmer. To the best of authors’ knowledge, there is no existing research on the turning behavior of marine animals. This article provides new insights into the turning strategies of dolphins, serving as a reference for future research.

## 2 Experiment Setup

The test field of the bottlenose dolphins (*Tursiops truncatus*) under observation resides in Dolphin Quest Oahu, HI. Animal care specialists train the dolphins to complete a regulated swimming task. A camera is set at a fixed position over the water surface, which allows the dolphins’ trajectory to be tracked at any position during the test trials.

Each experimental trial tests a single dolphin. The wearable device used is MTag [Lauderdale et al., 2021], a type of biologging tag designed to record the monitored animal’s kinematic and environmental data. Dolphins are trained to wear the MTags prior to the study. The MTags can be easily removed by animal care staff at any time without damaging the dolphin’s skin. Before the experiment, the researcher shakes the MTag to provide a time offset that matches the time series between the camera data and the MTag data. Then, the MTag is attached to the back of the observed dolphin.

The example lap trial procedure is shown in Fig. 1. During the experiment, dolphins are tasked with performing lap motions in an elliptical shape, with trainers assisting in managing the dolphins’ movements. In one test trial, a single dolphin completes several swimming laps along the same route within a designated time frame. Between each lap, the tester allows the dolphin about one minute of rest to help it recover from fatigue.

## 3 Methodology

This section details the methods employed for experiment setup and data analysis in our research. Data collection involves the use of camera-based detection throughout the test field, as well as a wearable device called MTag, which is attached to the dolphin being tested. A particle filter

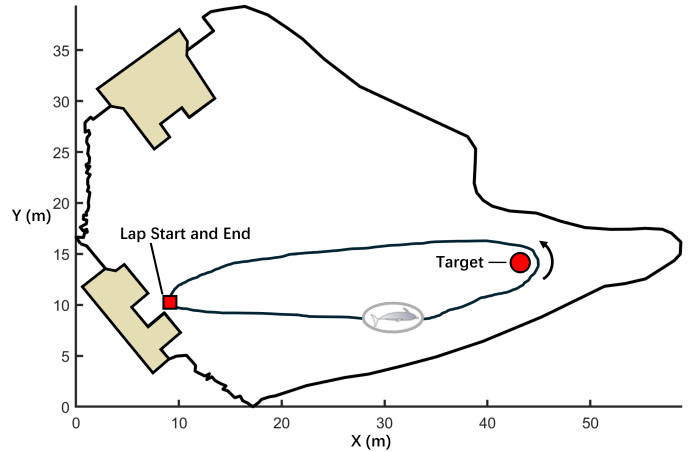


Figure 1: An example lap from an experimental trial. Trials consisted of 7 to 10 laps, with the dolphin starting from station and then swimming underwater around a target at the far end of the lagoon before returning to the starting position.

is applied to ensure a reliable trajectory. Furthermore, we develop a dynamic model based on the MTag data to analyze dolphin behavior.

### 3.1 Camera-based Detection

To identify the dolphin using camera data, a cutting-edge convolutional neural network known as faster region-based convolutional neural network (Faster R-CNN) [Ren et al., 2016] is employed for detection. This method consists of two primary components: a Region Proposal Network (RPN) and a Fast R-CNN detector network. The RPN identifies areas in an image that are likely to contain objects of interest and forwards these regions to the Fast R-CNN detector. The detector then verifies which of these regions truly contain the target objects. By integrating these two elements, a robust network is established that can effectively generate bounding boxes to pinpoint the location of objects within an image.

The Faster R-CNN detector is chosen for this study due to its superior precision compared to many single-shot detectors that prioritize speed. Additionally, the dolphins captured by the overhead camera vary significantly in pixel size. The Faster R-CNN detector is capable of recognizing the dolphins despite these size variations. Furthermore, the dolphins appear somewhat indistinct and lack detailed features, yet the Faster R-CNN demonstrates robust detection capabilities in these challenging conditions.

A pre-trained convolutional neural network, ResNet-50 [He et al., 2016], is chosen as the backbone for the Faster R-CNN detector. ResNet-50 is a 50-layer deep convolutional neural network (CNN). It has been pre-trained on over a million images. We utilize the version available in the Matlab Deep Learning Toolbox. The selection of the pre-trained ResNet-50 for this study is based on its optimal balance of accuracy and image processing speed. Furthermore, leveraging a pre-trained neural network through transfer learning is typically much faster and more straightforward than training a neural network from the ground up.

### 3.1.1 Training a Faster R-CNN Detector

The images used in this dataset are sourced from seven videos recorded in May 2024 in the lagoon on Oahu and have been carefully selected to highlight the unique characteristics of the dolphins. To minimize computational costs during training, the images have been cropped to a resolution of  $400 \times 400$  pixels, which corresponds to the largest size of a dolphin captured on video. Given that dolphins vary in size—from  $400 \times 400$  pixels down to  $50 \times 50$  pixels—the collection intentionally includes a range of dolphin sizes to ensure the detector can accurately identify them across different locations within the lagoon. Furthermore, the images depict dolphins observed under both optimal and suboptimal lighting conditions. Each image contains one or two dolphins and has been meticulously labeled using the Image Labeler tool within the Matlab Computer Vision toolbox, thereby providing the necessary ground truth data.

The labeled dataset is systematically divided into three distinct subsets: training, validation, and testing sets, consisting of 515, 50, and 56 images, respectively. The validation set plays a crucial role during the training phase by aiding in optimizing hyperparameters. In contrast, the testing set is utilized to assess the model’s performance after the training process is complete.

### 3.1.2 Verification of the Detector

The detector underwent initial evaluation using testing sets sized at  $400 \times 400$  pixels, achieving an average precision of 80.8% and a recall rate of 50.57%. However, since the detector is intended for tracking dolphins in a 4K video, more realistic testing is warranted. To facilitate this, a trial is conducted using footage recorded on May 13, 2024. During this trial, an image is extracted every two frames from the 20fps video, resulting in a total of 238 images. These images are then used to assess the performance of the trained detector through Matlab’s built-in function ‘evaluateObjectDetection’. When evaluated on the 4K dataset, the detector records an average precision of 49.4% and a recall rate of 34.58%.

### 3.1.3 Dolphin Detection

During detection, a threshold of 0.45 is established, representing the minimum confidence score required for a detection to be deemed valid. To focus specifically on the target dolphin, only detection results within the range of  $2150 < x < 3160$  and  $y < 1800$  are displayed, where  $x$  and  $y$  are measured in pixels. To eliminate false detections, only the results with the highest scores are retained. This approach is justified since there is only one dolphin of interest, and it is assumed that when the dolphin is clearly visible, the score associated with it is the highest, thus allowing for the exclusion of false detections.

### 3.1.4 Camera Calibration and Transformation

The position of each detected dolphin is adjusted to compensate for fisheye lens distortions using MATLAB’s Camera Calibration toolbox. A total of 173 images featuring a checkerboard pattern are utilized to calibrate the camera and assess the calibration results. The reprojection error

measures 0.83 pixels. Considering the images are captured at a resolution of  $3840 \times 2160$  pixels, this reprojection error is quite minimal, indicating a high level of precision in the calibration process. Subsequently, the corrected detections are transformed from the camera’s reference frame to the world reference frame using a perspective transformation homography [Hartley, 1997].

## 3.2 Tag-based Tracking

This section provides tag-based tracking in the 2D plane using the dead-reckoning method. The measurement of kinematic variables and equations of dead-reckoning is provided. Calculations are performed in the world reference frame.

### 3.2.1 Tag Kinematic Measurements

The MTag is equipped with various sensors, including an accelerometer, gyroscope, and magnetometer [Lauderdale et al., 2021]. The speed of the animal swimming through water is measured using a magnetic micro-turbine mounted outside the tag housing, along with a Hall effect sensor. Additionally, environmental temperature and pressure are also recorded. The angular velocity, acceleration, and geo-magnetism are recorded at a sampling rate of 50 Hz and are filtered with Madgwick filter [Madgwick et al., 2010], enabling the estimate of orientation. The depth and forward speed are recorded at a sampling rate of 5 Hz and are filtered with a method presented in [Gabalton, 2021].

Using the above kinematic variables, forward acceleration can be computed via the finite difference method. Prior to applying the finite difference method, the recorded linear speed is smoothed using the moving average technique to reduce noise. The normal acceleration is calculated using the equation provided below:

$$a_n = \omega v \quad (1)$$

Where  $a_n$  is the normal (centripetal) acceleration,  $\omega$  is the angular speed recorded using the MTag and  $v$  is the linear speed recorded using the MTag. Before calculating the normal acceleration, the linear speed and angular speed are all smoothed by taking the moving average to reduce noise.

### 3.2.2 Dead-reckoning

Dead reckoning [Wensveen et al., 2015] is a navigation technique employed to ascertain the position of a moving object by estimating its direction and distance traveled from a known starting point. This method involves continuously updating the position based on previously established locations, utilizing measurements of velocity, time, and direction of movement.

The following equation is used to update the position.

$$\vec{p}_{t+1} = \vec{p}_t + v\hat{n}\Delta t, \quad (2)$$

where  $\hat{n}$  is the unit heading vector,  $\Delta t$  is a short time calculated based on the sampling frequency,  $\vec{p}_t$  is the current position vector at time  $t$ , and  $\vec{p}_{t+1}$  is the position vector at time  $t + 1$ . The position vectors include the  $x$  and  $y$

positions of the dolphin, which are used to construct the dead-reckoning trajectory.

The method is designed to iterate from the initial position until the end of the dolphin’s lap. During each iteration, the current position is updated to reflect the next position derived from the previous iteration. The velocity is represented as a 2D magnitude, calculated by multiplying the velocity by the dolphin’s pitch angle. The heading vector is obtained from the MTag record. This approach assumes a steady speed and a constant heading within a small time interval.

### 3.3 Particle Filter Tracking

This section provides particle filter-based tracking in the 2D plane. A general description of the particle filter model is provided. We also demonstrate the mapping of the test field boundary and ground truth trajectory to show the particle filter’s performance. The calculations are performed in the world reference frame.

#### 3.3.1 Particle Filter Model

The tracking data collected for dolphins are MTag data and camera data. Both data sets can be used to plot the dolphin’s trajectory separately. However, the trajectories generated by the camera or tag alone are not reliable. A particle filter, a robust tool for estimating the state of a dynamic system from noisy observations, is used by combining the data from MTag and the camera.

The particle filter model applied is based on Zhang *et al.*’s model [Zhang *et al.*, 2019]. The probability distribution of states in the particle filter system is approximated by a cluster of weighted particles. The number of these particles is determined based on a trade-off between computational efficiency and estimation accuracy. Each weight indicates the reliability of the predicted trajectory. This model utilizes kinematic variables—such as speed, heading angle, and angular speed—from the MTag data, along with position data from the camera. It ultimately outputs the estimated track of the tested dolphin. Each state of the system encompasses the weight of all particles. Through the use of forward particle filtering, these states are propagated according to the provided dynamics model and external kinematic measurements (including both MTag and camera data), causing weight adjustments based on the reliability of the predicted trajectory. When the weight distribution of a state diverges significantly beyond a given threshold, the particle cluster undergoes resampling, resulting in the elimination of low-weight particles and the retention of high-weight ones for subsequent propagation. As all states are recorded throughout the process, a trajectory can be reconstructed for the entire experiment. It’s important to note that the forward particle filter determines states only using information from the past and present.

Non-causal particle filtering is employed to integrate future information into the state propagation process due to the limited confidence associated with the MTag measurements and camera data. However, if a particle is assigned more weight over time in the future, it can be assumed that this particle is carrying more reliable information in the past and present. Thus, only a portion of high-weighted

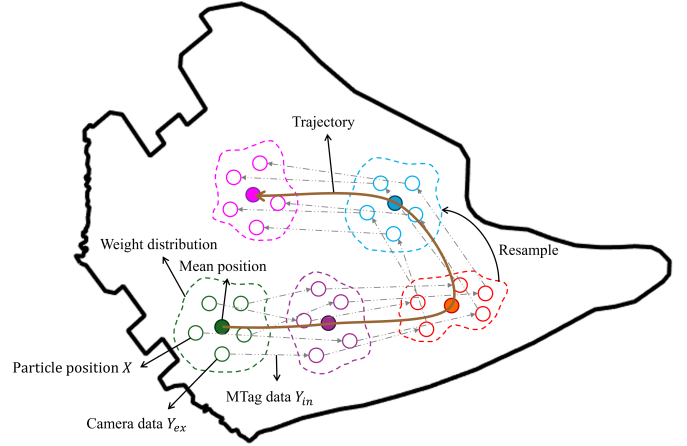


Figure 2: Diagram illustrating how the particle filter is used to estimate the location of the dolphin. Five states (solid green, purple, red, blue, and magenta circles), along with particle locations (open circles), along an estimated trajectory of the animal (brown line) from state to state. The dashed line denotes the weight distribution of the particles in a state. When the weight distribution exceeds a heuristically defined threshold, the particles will be resampled.

particles are selected to contribute to the dolphin’s trajectory in the non-causal particle filter, as the other particles might add inaccuracy. Note that all particles contribute to propagating the state forward. The non-causal particle filter won’t affect the process of the forward particle filter but only provides a more reliable state estimation. The trajectory of the observed dolphin is plotted to observe its behavior. Fig. 2 shows the propagation process of particles and Fig. 3 presents the structure of the implemented particle filter.

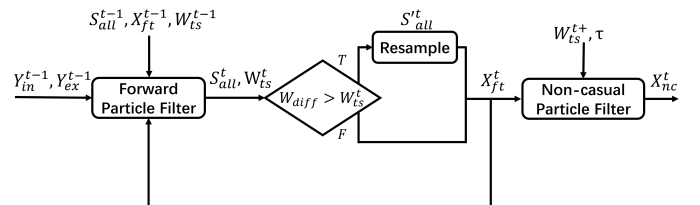


Figure 3: Block diagram of the particle filter. The process includes the Forward Particle Filter, the State Resampling Process, and the Non-Causal Particle Filter.  $t$  is the time step for the particle filter.  $Y_{in}^t$  denotes the internal measurement at time  $t$  from the MTag (speed, heading angle, and angular speed).  $Y_{ex}^t$  denotes the external measurement at time  $t$  from the camera (sparse position updates).  $W_{ts}^t$  denotes the heuristically defined weight difference threshold.  $S_{all}^t$  denotes the state of all the particles’ weight at time  $t$ .  $t_{rs}$  is the resampling time.  $X_{ft}^t$  denotes the predicted trajectory of the forward particle filter at time  $t$ .  $X_{nc}^t$  denotes the predicted trajectory of the non-causal particle filter at time  $t$ .  $\tau$  denotes the portion of particles selected for the non-causal particle filter.  $W_{diff}$  is the computed weight difference to verify if the current prediction of particle state is reliable.  $W_{ts}^{t+}$  represents the future information that helps determine a more precise trajectory.

### 3.3.2 Boundary Mapping

To establish a reference for the dolphins' location, it is essential to define the boundary of the lagoon. Initially, this boundary is created using Google Earth. Subsequently, the boundary data is imported into Matlab. Utilizing the Mapping Toolbox, the coordinates are converted from latitude and longitude into metric measurements.

### 3.3.3 Ground Truth Data Collection

Ground truth data plays a crucial role in assessing the accuracy of camera detection, dead-reckoning tracks, and particle filter tracks. To minimize manual effort and enhance the precision of the ground truth tracks, the video is downsampled from 20 Hz to 5 Hz, with the dolphin's position manually labeled in each frame. The dolphin's position is estimated as the geometric center. Following the manual labeling, the 5 Hz ground truth data is interpolated back to 20 Hz. The ground truth data is used to verify the reliability of the trajectory methods. We use the *mean error* to quantify the effectiveness of a trajectory:

$$\text{mean error} = \frac{\sqrt{(x - x') + (y - y')}}{n} \quad (3)$$

Where  $x$  and  $y$  denote the position of the trajectory,  $x'$  and  $y'$  denote the position of the ground truth data, and  $n$  denotes the number of sample points in a trajectory. A larger *mean error* shows a larger deviation from the ground truth data.

## 3.4 Tag-Based Modeling of the Swimming Biomechanics

This modeling approach is based on [Gabaldon et al., 2022b], and Fig. 4 illustrates the free-body diagram of the swimming dolphin.

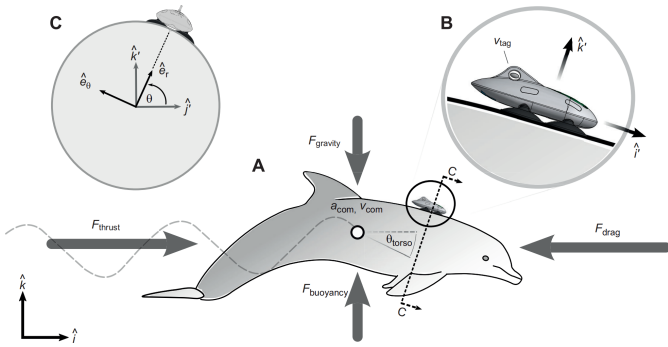


Figure 4: (A) Free-body diagram of a swimming dolphin. (B) A detailed view of the tag that illustrates the body-fixed reference frame of the tag/animal system and the speed sensor. (C) Cross-sectional view of the tag. The figure is referenced from Gabaldon et al. [2022b]

It is assumed that the dolphin balances the gravitational force by controlling its buoyancy. From the dynamic model, only the horizontal motion along the dolphin's movement is analyzed:

$$m' a_{\text{com}} = F_{\text{thrust}} + F_{\text{drag}} \quad (4)$$

Where  $a_{\text{com}}$  is the center-of-mass (COM) acceleration and  $m'$  is the total effective mass defined below:

$$m' = m + m_{\text{add}} \quad (5)$$

Where  $m$  is the mass of the animal and  $m_{\text{add}}$  is the added mass of fluid which is assumed to be  $m_{\text{add}} = 0.4 \rho V$  at the fluid density  $\rho = 1030 \text{ kg/m}^3$ . The drag force on the dolphin  $F_{\text{drag}}$  is defined by applying the depth-dependent drag model [Gabaldon et al., 2022b]:

$$F_{\text{drag}} = -0.5 \rho A_s C_D \gamma v_{\text{COM}}^2 \quad (6)$$

Where  $A_s = 0.08 m^{0.65}$  denotes the surface area,  $C_D = 16.99 Re^{-0.47}$  denotes the normalized drag coefficient [Fish, 1993],  $\gamma$  represents the depth-dependent coefficient [Hertel, 1966] accounting for wave drag when the animal swims near the surface, and  $v_{\text{COM}}$  is the center-of-mass velocity. The thrust power is defined by:

$$P_{\text{thrust}} = F_{\text{thrust}} v_{\text{com}} = \underbrace{m' a_{\text{com}} v_{\text{com}}}_{\text{Inertial}} - \underbrace{F_{\text{drag}} v_{\text{com}}}_{\text{Drag}} \quad (7)$$

Where  $F_{\text{thrust}}$  is the thrust force generated by the dolphin. By integrating the formulas mentioned above, we can derive the equation for thrust power:

$$P_{\text{thrust}} = \underbrace{(m + 0.4 \rho V) a_{\text{com}} v_{\text{com}}}_{\text{Inertial}} + \underbrace{0.5 \rho A_s C_D \gamma v_{\text{com}}^3}_{\text{Drag}} \quad (8)$$

The following formulas are used to present the predicted relationship between thrust power and linear velocity:

$$\hat{P}_{\text{thrust}}(v_{\text{com}}) = a_1 v_{\text{com}}^{a_2} \quad (9)$$

$$\hat{P}_{\text{t,nd}}(v_{\text{com}}) = b_1 (v_{\text{com}}/L)^{b_2} \quad (10)$$

Where  $a_1$ ,  $b_1$ ,  $a_2$ ,  $b_2$  are scalars calculated by non-linear curve fitting process and  $L$  is the dolphin's body length. These scalars are shown to be positive, resulting in a positive relationship for both thrust power and non-dimensional thrust power with linear velocity. The energetic cost during the dolphin's movement is defined as follows:

$$\text{COT} = \frac{P_{\text{thrust}} / (\eta_{ms} \eta_{sp}) + P_{\text{RMR}}}{m v_{\text{com}}} \quad (11)$$

Where  $P_{\text{RMR}}$  represents the metabolic power of the dolphin at rest,  $\eta_{ms} = 0.25$  represents the efficiency of converting chemical energy to mechanical energy in mammals [Massaad et al., 2007], accounting for energy loss during this process.  $\eta_{sp} = 0.85$  indicates the efficiency of converting internal power into external propulsive power allowing the movement in water. A predicted model of the cost is defined as follows:

$$\widehat{\text{COT}} = \frac{\hat{P}_{\text{thrust}}(v_{\text{com}}) / (\eta_{ms} \eta_{sp}(v_{\text{com}})) + P_{\text{RMR}}}{m v_{\text{com}}}, \quad (12)$$

where  $\widehat{\text{COT}}$  is the predicted energetic cost.

## 3.5 Normalization

As the dolphins navigate the corners, each trial is manually selected for analysis. The time series plots reveal similar behaviors among the dolphins, which facilitate the

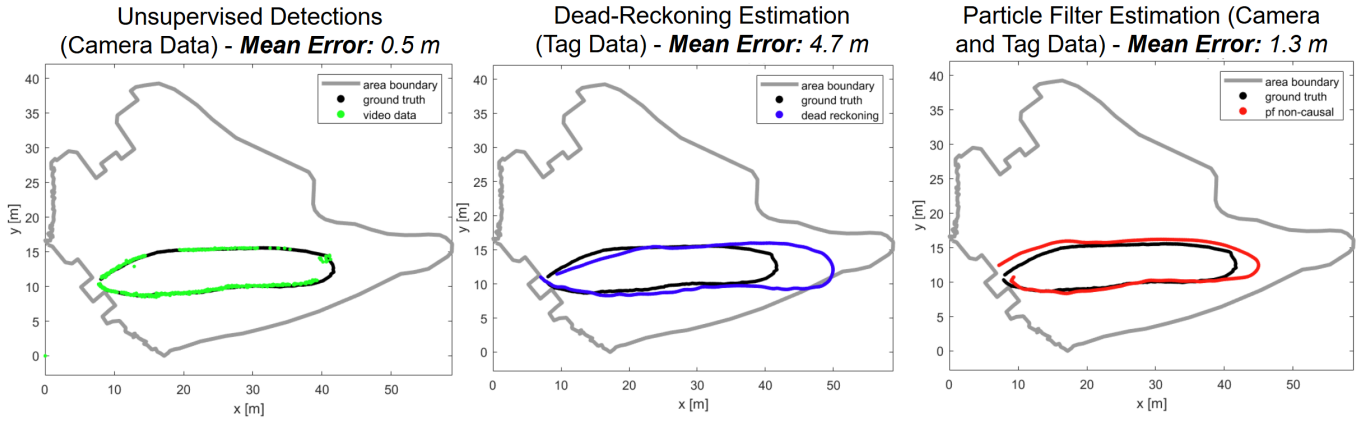


Figure 5: A comparison of the camera and tag-based localization estimates for a single lap. Supervised tracking is used to generate ground truth data (Black) presented in the three figures. **Left:** A comparison between the unsupervised detection results and the ground truth track. **Middle:** The dead-reckoning location estimate calculated from tag data. **Right:** Results from the particle filtering approach that uses both tag and camera data. Supervised tracking is used to generate ground truth data (Black) presented in the three figures.

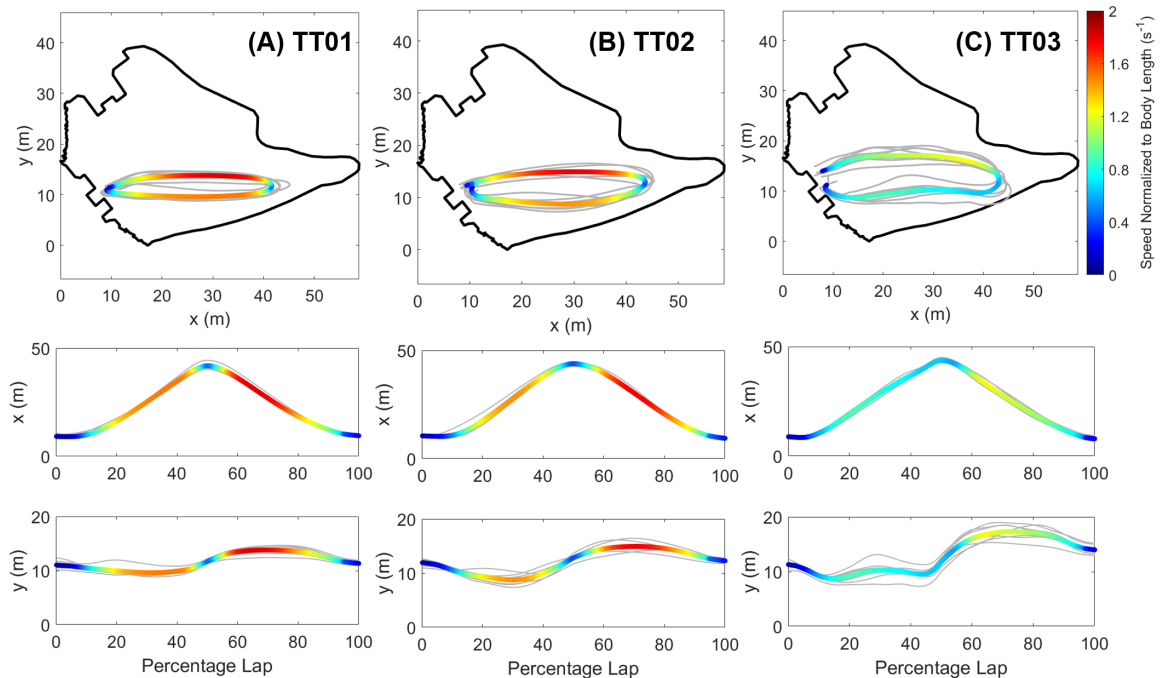


Figure 6: Estimated path and measured speed during the lap swimming trials. Individual (grey lines) and trial average paths are presented along with the average lap speed (heat map). Speed was normalized to body length.

normalization process. It is assumed that when the normal acceleration reaches its maximum value, the dolphin has completed half of the turn, marking the 50% lap point. Following this, the laps from 0 to 50% and from 50% to 100% percent are normalized separately to effectively represent the dolphins' behaviors.

The dolphin's speed is normalized to body length by dividing the speed of the dolphin by the body length for comparison between dolphins with different properties (lengths and masses):

$$v_{\text{normal}} = v_{\text{com}}/L \quad (13)$$

Where  $v_{\text{normal}}$  is the speed normalized to body length (body-length speed). Thrust power is also normalized to a non-dimensional form  $P_{t,nd}$  to make comparisons between dolphins with different properties (lengths and masses):

$$P_{t,nd} = P_{\text{thrust}} / (mg^{1.5}L^{0.5}) \quad (14)$$

Where  $g$  is the gravitational acceleration equal to  $9.81 \text{ m/s}^2$ .

## 4 Results

This section presents experimental data and tracks the swimming behavior of dolphins. We compare the trajectory results generated by MTag data, camera detection, and a particle filter to assess the reliability of the particle filter model. The normalized particle filter trajectories of the tested dolphins are used to study their corning strategies. The kinematic variables collected by MTag are shown in a time series alongside event detection. These analyzed kinematic variables are normalized to provide clearer insights into dolphin behavior.

## 4.1 Verification of the Particle Filter Based Tracking

Before using the particle filter to analyze the dolphin's behavior during cornering, the trajectory generated by the model is compared to the camera-based trajectory and the dead-reckoning trajectory. The comparison is shown in Fig. 5.

## 4.2 Normalized Particle Filter Trajectory

The particle filter provides a trajectory for each dolphin's test trial. Speed is quantified by normalizing to body length. The position normalized to percentage lap is plotted for a deeper insight into the distance the dolphin travels. The trajectories are shown in Fig. 6.

The average radius of curvature at the corner is calculated to analyze the cornering behavior of the tested dolphins in Fig. 7.

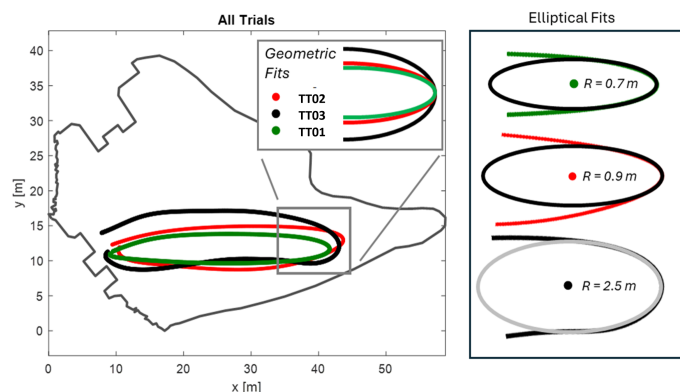


Figure 7: A comparison of the trajectory between different dolphins. Dolphin TT03 travels the longest distance with a big turning radius. Dolphin TT02 travels a distance shorter than Dolphin TT03 with a sharp turn when cornering. Dolphin TT01 travels the shortest distance with a sharp turn when cornering.

## 4.3 Time Series Plot for Lap Trials

To provide an overview of a set of continuous lap trials, the time series plot is presented in Fig. 8. The plots display depth, linear speed, forward acceleration, roll angle, pitch angle, yaw angle, normal acceleration, thrust force power, and cost of transport (COT) for dolphin TT02.

From the time series plot, one lap is manually extracted to identify the events during the trial: starting, cornering, and ending. The event detection is illustrated in Fig. 9

## 4.4 Normalize to Percentage Lap

To analyze the energetic costs and strategies dolphins adopt when turning, we plot the values of key kinematic variables in percentage lap in Fig. 10, and compare the difference between the three tested dolphins in Fig. 11.

## 4.5 Motion and Energetic Analysis

A box plot is provided for each dolphin to show the work consumption during different events in lap swim. For each plot, the work for the whole lap is divided into transient

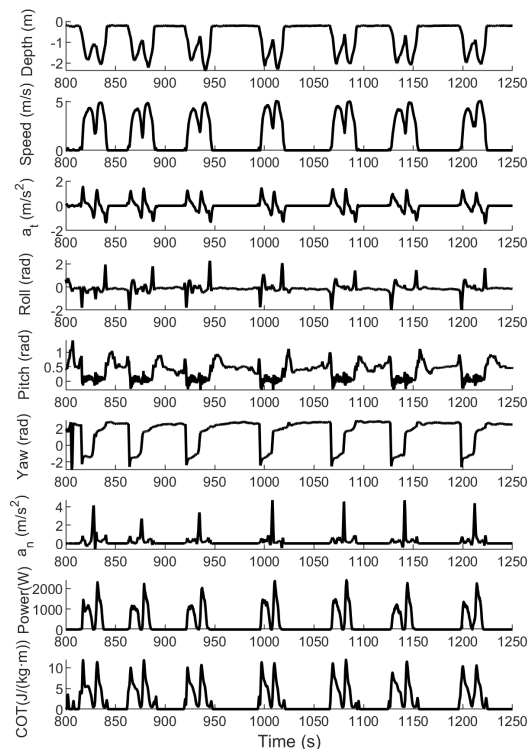


Figure 8: Measured and calculated kinematic variables plotted as a time series for dolphin TT02.

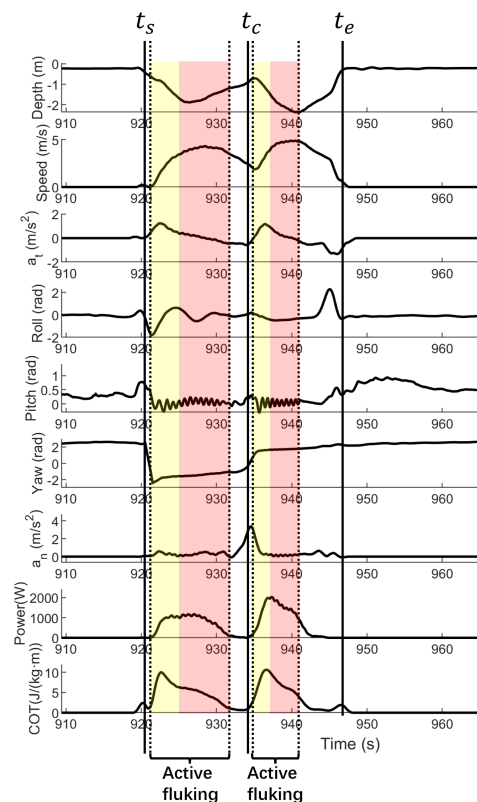


Figure 9: Measured and estimated kinematic data for dolphin TT02 from a lap. Features in the data were used to identify: 1) lap start ( $t_s$ ), 2) the cornering event ( $t_c$ ), and 3) lap end ( $t_e$ ). The yellow shading denotes the transient period of swimming, and the red shading denotes the consistent speed period. The animal flukes actively during both transient and consistent speed periods.

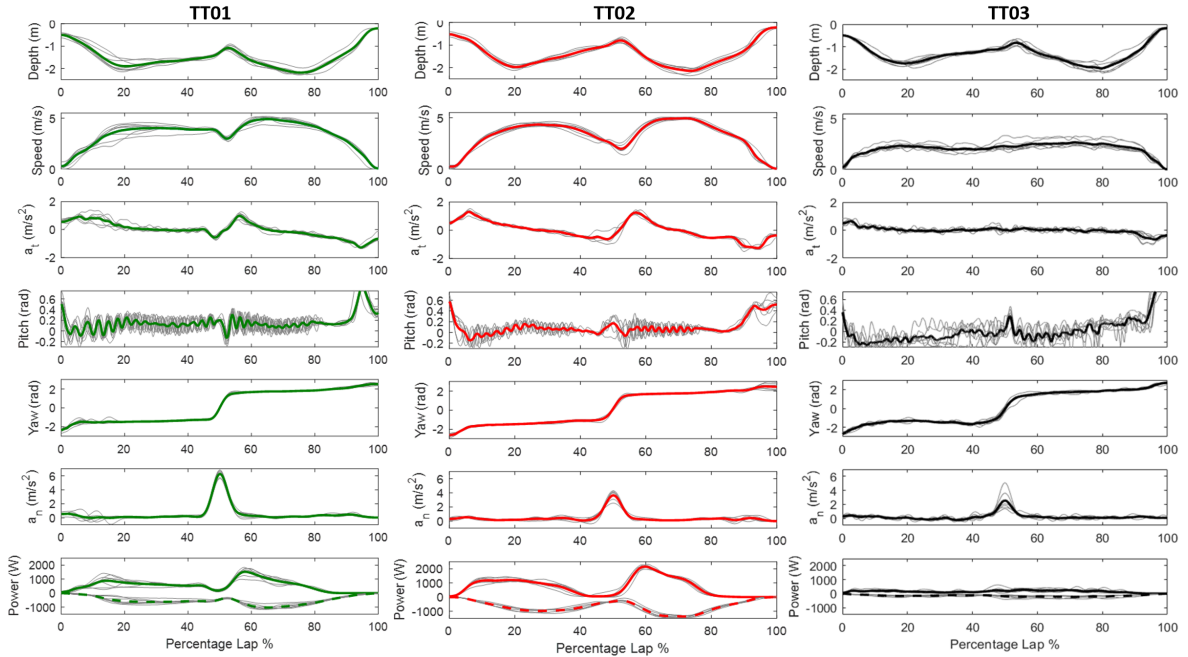


Figure 10: Key kinematic (depth, speed, acceleration, and orientation) and kinetic (thrust power) parameters from the animals. Data are normalized to percentage lap, and the cornering event occurs at 50% of the lap. The individual (grey lines) and average (colored bolded line) data for the results are presented in each sub-figure.

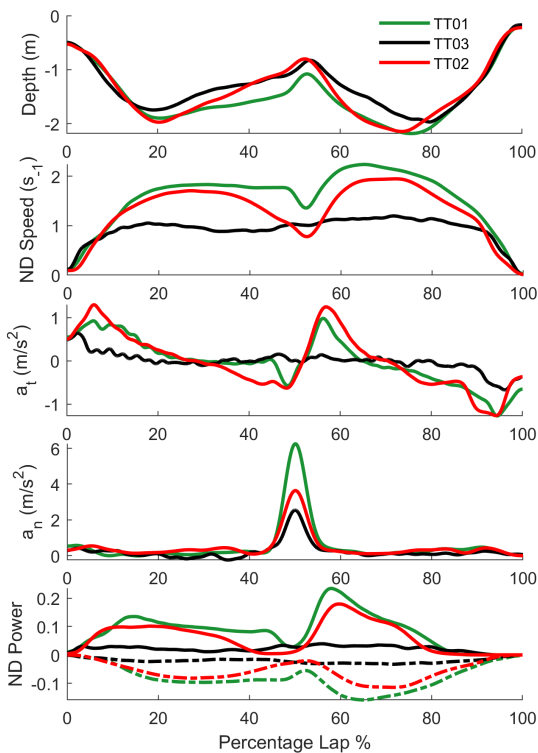


Figure 11: A comparison of average kinematic (depth, speed, and acceleration) and kinetic parameters (drag and thrust power). Thrust power is positive (solid lines) and drag power is negative (dashed lines) for the three animals.

swimming and steady-state swimming. The box plots are shown in Fig. 12.

## 5 Discussion

This section analyzes our research findings. The particle filter model has proven to be the most reliable tracking method compared to tag-based dead-reckoning tracking and camera-based detection. We also explore the swimming behaviors of various dolphins.

### 5.1 Verification of the Particle Filter Based Tracking

In the trajectory obtained from the camera, as illustrated in Fig. 5, the detected positions of the dolphins are close to the ground truth, achieving a mean error of 0.51 meters. This indicates that the trained Faster R-CNN detector can precisely identify the dolphins. However, there are instances where the trajectory is incomplete due to the detector's inability to identify the dolphins. This missed detection is primarily attributed to the glitter on the water's surface, which adversely affects the detector's performance. Additionally, in some cases, the dolphins are submerged and not even visible to the naked eye. Moreover, the detection from the camera is noisy.

In the dead-reckoning trajectory illustrated in Fig. 5, the dolphin appears to venture far into the lagoon and even collides with the boundary, which is a scenario unlikely to occur in real-world conditions. The norm of mean estimation error between the dead-reckoning trajectory and the ground truth is 4.76 meters, which is larger than the estimation errors from the particle filter. This larger error can be attributed to the fact that each position in the dead-reckoning trajectory is determined based on the preceding position. Given that speed measurements are prone to noise, this introduces errors in the positioning. As the dolphin swims further away, these positional errors accumulate, ultimately resulting in a greater overall error in the trajectory. Additionally, the velocity sensor captures



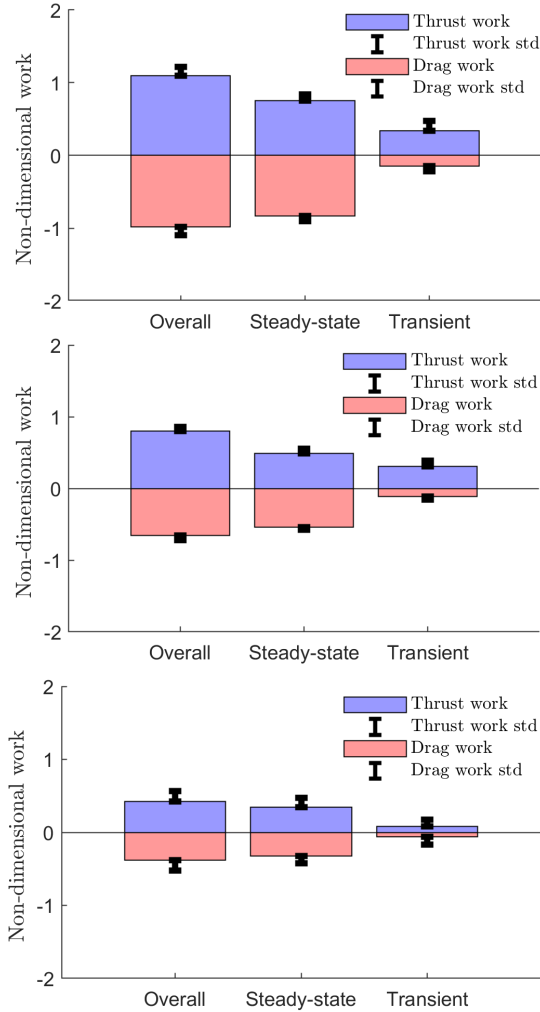


Figure 12: Non-dimensional work calculated from the thrust and drag power for each dolphin calculated during: active fluking, transient swimming, and consistent speed swimming. The work during active fluking is the sum of the work done by the animal during the transient and consistent speed swimming.

the relative speed between the water and the dolphin. If the dolphin swims against the current, the recorded speed will exceed its actual speed, further contributing to inaccuracies in the trajectory.

The particle filter demonstrates a smooth and comprehensive trajectory of the dolphin's swimming behavior. The mean error associated with the particle filter trajectory is 1.27 meters. In comparison to the dead-reckoning method, this trajectory exhibits a more minor deviation from the ground truth, resulting in a more reliable representation of the dolphin's underwater activities. When contrasted with the trajectory recorded by the camera, the particle filter's trajectory is slightly less precise, as it deviates more from the ground truth. This discrepancy may be attributed to the design's heavy reliance on tag data. Nonetheless, the particle filter guarantees that the trajectory remains continuous and complete. It can track the dolphin even when it can not be seen in the video. Furthermore, the trajectory produced by the particle filter displays considerably less noise than the camera-generated trajectory, offering a clearer depiction of the swimming route.

With the application of the particle filter, we are con-

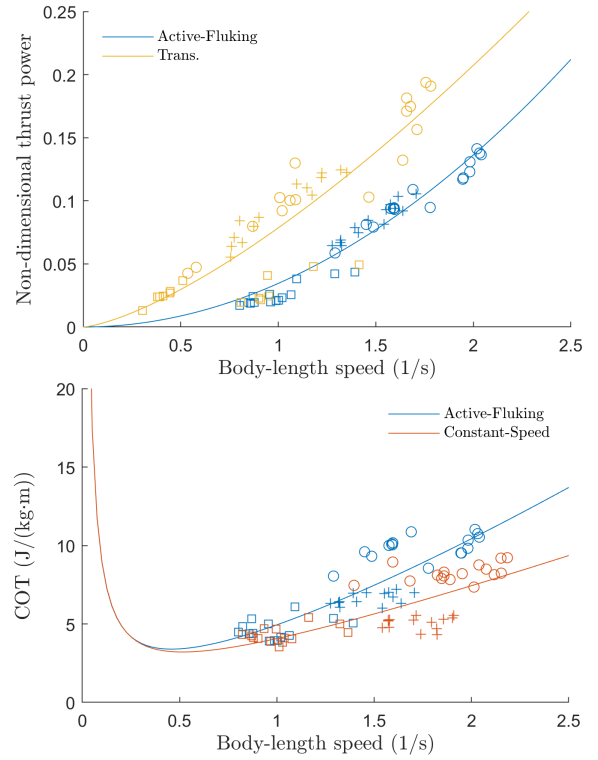


Figure 13: **Top:** A comparison of the estimated power generated by the animals during transient and consistent speed swimming: TT1 (Circles), TT2 (Plus Marks), and TT3 (Square). The animals generated more power during transient swimming. **Bottom:** Cost of transport calculated during swimming (active fluking) compared to COT during steady speed swimming.

fident in delivering a reliable trajectory of the dolphin's underwater swimming behavior, with all positions accurately recorded.

## 5.2 Motion and Energetic Analysis

In Fig. 6, the trajectory and speed of the three dolphins are displayed. It can be observed that the dolphins swim faster during the last half of the lap trials. At the corner, TT02 and TT01 slow down, while TT03 maintains its speed. In Fig. 7, the average radius of curvature is shown. TT03 presents a larger turn while TT01 and TT02 choose a small, sharp turn at the expense of reducing their speed.

The time series plot in Fig. 8 shows that the tested dolphin performs similarly in every lap trial. This allows for event detection and ensures that the average lap data can represent the dolphin's overall behavior.

The normalized kinematic variables from the MTag data, illustrated in Fig. 10 and Fig. 11, reveal the swimming preferences of the dolphins. Dolphin TT01 and TT02 exhibit faster swimming motions, reaching a maximum speed of 5 m/s, while dolphin TT03 swims at a comparatively slower pace, with a maximum speed of 1.8 m/s.

The cornering strategies of the three tested dolphins are compared in terms of normalized speed, normalized thrust power, and cost of transport (COT). Among the three dolphins, TT03 exhibits the lowest work consumption, power output, and COT. This indicates that TT03 incurs the least energetic cost during cornering. The efficiency of TT03 can be attributed to its slower and constant

swimming speed, which is maintained even while cornering. Analysis of the non-dimensional work plot indicates that the thrust work performed by TT03 occurs mostly at a constant speed, with 80.82% of the total thrust work being done during this constant speed interval. Consequently, TT03 demonstrates the most efficient swimming, utilizing the least energy cost. From the normalized speed plot shown in Fig. 11, it is evident that both TT01 and TT02 swim faster than TT03. However, TT01 exhibits the fastest average speed, making it the quickest among the three dolphins. This speed is achieved by maintaining speed during cornering and spending more time swimming in the steady state. However, TT01 has a higher non-dimensional power and a higher COT, indicating that it needs more power to move at a higher speed. In contrast, although TT02 swims slower than TT01, it uses less power. Additionally, TT02 demonstrates a significantly lower cost of transport (COT) compared to TT01, indicating greater efficiency. Notably, TT02 is the heaviest of the three dolphins, so it is efficient at moving a larger weight.

From the box plot of work consumption shown in Fig. 12, TT01 performs the highest thrust work due to its fast speed. However, the steady-state swim of TT01 takes about 68.85 % of the overall work, which is larger than TT02 (61.34%). This indicates that TT01 spends more work during steady-state swimming.

From the figures of the energy analysis shown in Fig. 13, the fit of the non-dimensional thrust power curve exceeds the active-fluking (overall) thrust power. Moreover, it is shown that COT at constant speed is smaller than active-flucking (overall) COT. By combining the observations from the two figures, dolphins can save more energy by using their energy during constant-speed swimming. TT01 remains at constant-speed swimming at high speed and saves energy for performing sharp turns.

### 5.3 Limitations

The Faster R-CNN detector described in Section 3 has occasional object mis-classification problem, which can be resolved by introducing an additional classifier. To this end, we restrict the detection area to the water area since there are no active individuals in the lagoon. Moreover, glare on the water’s surface negatively affects the detector’s performance. The effectiveness of the detector is also impacted by lighting conditions. Since the videos are captured outdoors, the water in the lagoon often appears very dark, making it difficult to see anything underwater, even with the naked eye. To enhance accuracy and achieve more comprehensive tracking, it is recommended to conduct tests around midday, as this can help reduce shadowing on the lake.

Moreover, due to the limited number of test samples, we can only conclude the article with qualitative conclusions.

## 6 Conclusion

In this article, a Faster R-CNN detector is trained for the detection and localization of dolphins. A particle filter is utilized to combine data from both the camera and tags, effectively constructing the trajectories of the dolphins tested. By comparing the trajectories generated by

the particle filter with those obtained through camera-based, tag-based tracking and the ground truth trajectories, particle filter shows stronger robustness. Additionally, a dynamic model from existing research is employed to quantify the thrust force for energetic analysis. Utilizing kinematic measurements from the tags alongside the trajectories produced by the particle filter, the swimming performance of three tested dolphins is assessed. TT01 emerges as the fastest lap swimmer, achieving the highest overall speed while executing sharp turns with small deceleration. TT02 demonstrates greater energy efficiency than TT01 by transferring more weight at high speeds. Meanwhile, TT03 exhibits the highest energetic efficiency by maintaining slow speeds.

Future work includes the implementation of larger dataset for statistical analysis of the dolphin’s corning behavior. A path-planning strategy that minimizes the energetic cost when turning will be summarized.

## Acknowledgments

The authors would like to thank the Dolphin Quest Oahu for the aid in facilitating this research.

## References

- G. Antoniak, E. Xargay, J. Gabaldon, K. Barton, B.-I. Popa, and K. A. Shorter. Estimating propulsive efficiency of bottlenose dolphins during steady-state swimming. In *2023 IEEE Conference on Control Technology and Applications (CCTA)*, pages 675–680. IEEE, 2023.
- F. E. Fish. Power output and propulsive efficiency of swimming bottlenose dolphins (*tursiops truncatus*). *Journal of Experimental Biology*, 185(1):179–193, 1993.
- F. E. Fish and J. Rohr. Review of dolphin hydrodynamics and swimming performance. 1999.
- F. E. Fish, P. Legac, T. M. Williams, and T. Wei. Measurement of hydrodynamic force generation by swimming dolphins using bubble dpiv. *Journal of Experimental Biology*, 217(2):252–260, 2014.
- J. Gabaldon. *Contextualized Monitoring in the Marine Environment*. PhD thesis, 2021.
- J. Gabaldon, D. Zhang, K. Barton, M. Johnson-Roberson, and K. A. Shorter. A framework for enhanced localization of marine mammals using auto-detected video and wearable sensor data fusion. In *2017 IEEE/RSJ International Conference on Intelligent Robots and Systems (IROS)*, pages 2505–2510. IEEE, 2017.
- J. Gabaldon, D. Zhang, L. Lauderdale, L. Miller, M. Johnson-Roberson, K. Barton, and K. A. Shorter. Computer-vision object tracking for monitoring bottlenose dolphin habitat use and kinematics. *PloS one*, 17(2):e0254323, 2022a.
- J. T. Gabaldon, D. Zhang, J. Rocho-Levine, M. J. Moore, J. Van der Hoop, K. Barton, and K. A. Shorter. Tag-based estimates of bottlenose dolphin swimming behavior and energetics. *Journal of Experimental Biology*, 225(22):jeb244599, 2022b.
- R. I. Hartley. In defense of the eight-point algorithm. *IEEE Transactions on pattern analysis and machine intelligence*, 19(6):580–593, 1997.
- K. He, X. Zhang, S. Ren, and J. Sun. Deep residual learning for image recognition. In *Proceedings of the IEEE conference on computer vision and pattern recognition*, pages 770–778, 2016.
- H. Hertel. Structure form movement. *English Language Edition*, 1966.
- A. Kaidarova, N. R. Gerdali, R. P. Wilson, J. Kosel, M. G. Meekan, V. M. Eguíluz, M. M. Hussain, A. Shamim, H. Liao, M. Srivastava, et al. Wearable sensors for monitoring marine environments and their inhabitants. *Nature Biotechnology*, 41(9):1208–1220, 2023.
- L. K. Lauderdale, K. A. Shorter, D. Zhang, J. Gabaldon, J. D. Mellen, M. T. Walsh, D. A. Granger, and L. J. Miller. Bottlenose dolphin habitat and management factors related to activity and distance traveled in zoos and aquariums. *PloS one*, 16(8):e0250687, 2021.
- S. Li, Z. Wu, J. Wang, C. Qiu, M. Tan, and J. Yu. Robust depth and heading control system for a novel robotic dolphin with multiple control surfaces. *IEEE Transactions on Automation Science and Engineering*, 2024.
- S. Madgwick et al. An efficient orientation filter for inertial and inertial/magnetic sensor arrays. *Report x-io and University of Bristol (UK)*, 25:113–118, 2010.
- F. Massaad, T. M. Lejeune, and C. Detrembleur. The up and down bobbing of human walking: a compromise between muscle work and efficiency. *The Journal of physiology*, 582(2):789–799, 2007.
- S. Ren, K. He, R. Girshick, and J. Sun. Faster r-cnn: Towards real-time object detection with region proposal networks. *IEEE transactions on pattern analysis and machine intelligence*, 39(6):1137–1149, 2016.
- P. J. Wensveen, L. Thomas, and P. J. Miller. A path reconstruction method integrating dead-reckoning and position fixes applied to humpback whales. *Movement ecology*, 3:1–16, 2015.
- R. P. Wilson, K. A. Rose, R. S. Metcalfe, M. D. Holton, J. Redcliffe, R. Gunner, L. Börger, A. Loison, M. Jezek, M. S. Painter, et al. Path tortuosity changes the transport cost paradigm in terrestrial animals. *Ecography*, 44(10):1524–1532, 2021.
- J. Yu, Z. Wu, Z. Su, T. Wang, and S. Qi. Motion control strategies for a repetitive leaping robotic dolphin. *IEEE/ASME Transactions on Mechatronics*, 24(3):913–923, 2019.
- D. Zhang, J. Gabaldon, L. Lauderdale, M. Johnson-Roberson, L. J. Miller, K. Barton, and K. A. Shorter. Localization and tracking of uncontrollable underwater agents: Particle filter based fusion of on-body imus and stationary cameras. In *2019 International Conference on Robotics and Automation (ICRA)*, pages 6575–6581. IEEE, 2019.
- D. Zhang, Y. Wang, J. Gabaldon, L. K. Lauderdale, L. J. Miller, K. Barton, and K. A. Shorter. Dynamics and energetics of bottlenose dolphin (*tursiops truncatus*) fluke-and-glide gait. *Journal of Experimental Biology*, 226(15), 2023.